Macromolecules

Article

pubs.acs.org/Macromolecules

Diffusion and Permeation of Labeled IgG in Grafted Hydrogels

A. Vagias,[†] K. Sergelen,[‡,§] K. Koynov,[†] P. Košovan,[∥] J. Dostalek,[‡] U. Jonas,[⊥] W. Knoll,[‡] and G. Fytas*[,†]

[†]Max Planck Institute for Polymer Research, Ackermannweg 10, 55128 Mainz, Germany

[‡]Biosensor Technologies, AIT-Austrian Institute of Technology GmbH, Muthgasse 11, Wien 1190, Austria

[§]International Graduate School on Bionanotechnology, University of Natural Resources and Life Sciences, Nanyang Technological University, Singapore 639798

[∥]Department of Physical and Macromolecular Chemistry, Faculty of Science, Charles University, Prague, Czech Republic

[⊥]Macromolecular Chemistry, Department Chemistry - Biology, University of Siegen, 57076 Siegen, Germany

Supporting Information

ABSTRACT: The permeation and translational diffusion of antibodies through the porous matrix of hydrogel materials is of fundamental relevance for many biological systems in living nature, but equally important in medical and technological applications, such as implanted drug release systems and biosensors. In this respect the diffusion of fluorophore-labeled protein immunoglobulin G (IgG) in micrometer thick, grafted hydrogel layers based on thermoresponsive poly(*N*-isopropylacrylamide) (pNiPAAm) is studied here by fluorescence correlation spectroscopy (FCS). The pore size of the gel gradually changes with its swelling state, which is controlled by the cross-link density of the network, temperature, and pH value of the surrounding medium. Notably, IgG permeation in these hydrogel layers exhibits a much more complex dependence on these factors. This rich variability of IgG permeation is attributed to the varying balance of protein interactions with the polymer network through electrostatics, controlled pH-dependent protein ionization, excluded volume repulsion, and hydrophobic attraction. A combined analysis of the fluorescence intensity profiles and the dynamics monitored by FCS allows us to quantify the thermodynamically controlled partitioning of IgG as well as the slowdown of its diffusion. Contrary to the complex behavior of the permeation, the diffusion slowdown seems to be a universal function of polymer volume fraction, which is rather robust with respect to temperature or pH changes. The presented findings suggest a model approach to explore the synergy between crowding and thermodynamics with respect to the controlled protein transport in pNiPAAm-based hydrogels.

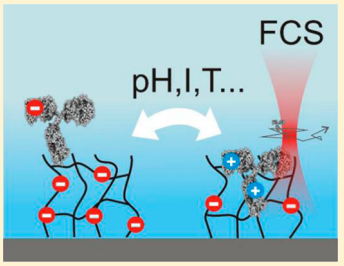

INTRODUCTION

Polymer networks that form hydrogels become irreplaceable building blocks in diverse fields ranging from actuators[1,2] to shape memory[3,4] and self-healing materials,[5−7] and they rapidly find applications in the biomedical domain for tissue engineering,[8,9] drug delivery,[10] implants, and wound dressings[11,12] as well as in analytical technologies for the biomarker analysis present in complex biological samples.[13−15] In particular, the biomedical areas take advantage of hydrogel architectures with tailored interaction and transport of biomolecules through the polymer networks. For instance, responsive hydrogels can be designed to serve as inert antifouling materials[16,17] or as systems for on-demand capture or release of specific biomolecules.[18,19] In the analytical field, numerous biosensor technologies rely on hydrogel materials attached at the interface between a physicochemical transducer and the analyzed liquid sample.[20−24] Such an interfacial architecture is typically engineered to suppress fouling of the sensor surface by unspecific binding of a large number of different molecules abundantly present in the analyzed sample. Furthermore, the hydrogel layer can serve to accommodate large density of ligands that are accessible for specific capture of target analyte while allowing efficient transport of target analyte in and out of the networks. The transport of analytes through such networks is frequently diffusion-limited.[25,26] Hence, the design features of such hydrogel-based sensors are univocally expected to be dictated by a large number of factors, such as size of target analyte, hydrogel pore size, polymer volume fraction, temperature, ionic strength, and pH in the case of charged hydrogels as well as various interactions with solute.[27−30] The complex interplay of these parameters strongly affects the solute transport and adsorption in the bulk gel network, which needs to be stringently controlled in order to efficiently utilize hydrogels in analytical devices. So far, a complete predictive correlation between solute diffusion dynamics and stimulus-responsive structural features of the hydrogel has remained elusive.

Thus, the synergy between the gel network structure and the underlying tracer−network interactions that take place in contact with complex biological samples in aqueous media render the exact elucidation of tracer dynamics rather nontrivial. Earlier fluorescence correlation spectroscopy (FCS) studies have focused on the molecular tracer diffusion dynamics in hydrogels[28,31−33] as a function of cross-link

Received: March 9, 2017
Revised: May 29, 2017

DOI: 10.1021/acs.macromol.7b00514
Macromolecules XXXX, XXX, XXX−XXX

density, polymer volume fraction, temperature, and the mechanical and dynamic properties of the grafted hydrogel layers.[34−36] However, a multivariable investigation on the combined influence of external parameters including temperature, cross-link density, and buffer condition that affects dynamics of biomolecular solutes transport in hydrogel structure still remains an unexplored intriguing task. Successful decoupling the impact of each factor on either the biomolecule penetration and/or dynamics may provide clues for efficient control of hydrogel functionality in numerous applications. Potentially, the gained fundamental understanding can aid the efficient design of separation membranes and novel sensors[37−46] or chromatographic setups[47−50] where binders of variable affinity strength[51−63] toward the matrix can be encountered.

Our biosensor-inspired motivation for this work stems from the need to optimize the design of hydrogel-based affinity binding matrices employed in fluorescence sensors specifically to IgG, which represents an important class of large molecular-weight proteins that are employed in the vast majority of assays for detection of chemical and biological species. Studies on diffusion of large macromolecular tracers such as IgG in numerous types of hydrogels have been reported.[25,30,64−71] Because of their versatility and commercial availability, IgGs are employed in numerous types of fluorescence immunoassays and are either directly coupled to a polymer binding matrix (e.g., capture antibody) or they are labeled with fluorophores and affinity-bound at the surface (e.g., detection antibody in sandwich immunoassay).[15,22,72] In addition, IgGs can serve as biomarkers of various diseases[73−75] and as drugs.[76,77]

By applying the FCS method to thin surface-attached hydrogel films, two features of the measurements can be exploited: (1) By recording the static fluorescence signal while scanning the confocal probing volume (focal spot) perpendicular to the substrate surface through the hydrogel layer and adjacent medium (termed z-scan), the distribution of the fluorescent markers within the gel and in relation to the free molecules in solution can be determined. (2) By time correlation of the fluorescence intensity signal within the hydrogel medium the dynamic components can be analyzed, which provides detailed information about dynamic inhomogeneities and potential interactions between the fluorescent molecules and the hydrogel network depending on the condition (e.g., temperature) and medium composition (e.g., salts and pH). Using FCS, we examined the influence of cross-link density, polymer volume fraction, temperature, and composition of buffer in which a pNiPAAm-based hydrogel layer is swollen on the diffusion dynamics of IgG biomolecules. The single-molecule sensitivity (nanomolar tracer concentration) of the FCS method[78] provides conditions that are approaching the real-time analyte detection limit in gel-based biosensors.[24] In addition, the method is better suited for detection of reaction kinetics of weak affinity binders as compared to surface plasmon resonance methods[79] or to the more indirect chromatographic techniques.[49] The results are discussed in view of diffusion slowdown measurements and estimations of local partition coefficients for IgG in the hydrogel phase. The paper is outlined as follows: The results on the swelling of pNiPAAm hydrogels in used buffers at different temperatures and the IgG permeation in these hydrogels are discussed in subsection A. Discussion of the diffusion dynamics of the labeled IgG inside such hydrogel architectures is presented in subsection B. The preparation of samples and the FCS technique are presented in the Experimental Section.

RESULTS AND DISCUSSION

A. Hydrogel−Protein Interactions. The distribution of IgG molecules labeled with Alexa Fluor 647 dye (A647) was investigated in hydrogel films with different cross-linking density. The films were prepared from photo-cross-linkable poly(N-isopropylacrylamide)-based polymer (pNiPAAm) by irradiation with UV light for 5min (XL-5), 10 min (XL-10), and 15 min (XL-15) with UV light.[80] These surface-attached hydrogel films on glass substrates were swollen in solutions of the IgG−A647 conjugate dissolved either in phosphate buffered saline (PBS) with a pH of 7.4 or in acetate buffer (ACT) with pH 4. As seen in the z-scan of Figure 1, the hydrogel layers

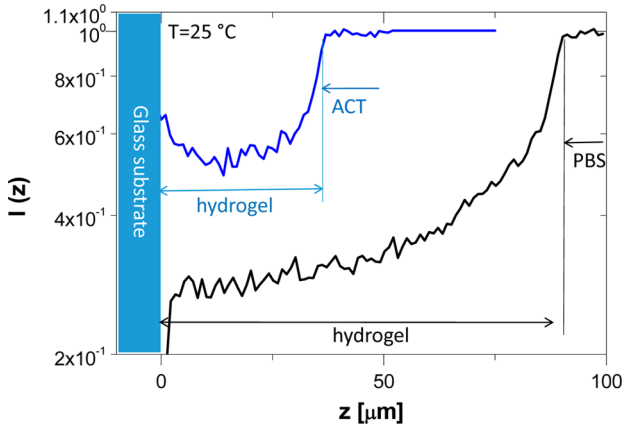

Figure 1. Z-scan through a hydrogel layer with normalized fluorescence intensity $I(z)$ measured as a function of distance z normal to the glass substrate with attached hydrogel layer (hydrogel XL-5, Table 1) swollen at T = 25 °C in PBS (pH = 7.4, black) and acetate buffer (ACT, pH=4, blue).

exhibit distinct swelling ratios for the different pH (about twice at pH = 7.4 in PBS compared to pH = 4 in acetate at 25 °C). The z-scan depicts the spatial distribution of time-averaged fluorescence intensity, $I(z)$, of the A647-labeled IgG (large tracer) and the coexistent small amount of free A647 in the direction normal to the substrate. Small A647 molecules are present in very low amount as residual species from the labeling process, which can be identified by their fast diffusion characteristics (as measured by time correlation and discussed below).

The z-scan shows the two boundaries of the hydrogel: one to the glass substrate (z = 0) and one to its outer surface in contact with the liquid medium. Inside the hydrogel layer, the intensity of fluorescence signal $I(z)$ is lower than that in the liquid medium due to the hindered penetration of A647-labeled IgG. The outer interface is manifested as the distance z from the glass surface beyond which the fluorescence intensity $I(z)$ is constant. From the experimental $I(z)$ profiles, the polymer volume fraction ϕ was determined as the ratio of the dry layer thickness to the swollen layer thickness for all combinations of hydrogel cross-linking density XL, temperature, and buffer, as specified in Table 1. The experimental swelling ratio R_s is defined as the inverse of the polymer volume fraction ϕ^{-1}. Three distinct effects can be discriminated from the analysis of the z-scan data: (I) the swelling ratio, (II) the tracer

DOI: 10.1021/acs.macromol.7b00514
Macromolecules XXXX, XXX, XXX−XXX

Table 1. Values for the Polymer Volume Fraction $\phi(T)$ (±10%) of the Different PNiPAAm Hydrogel Layers Examined (Swollen in ACT or PBS) for the Respective UV Irradiation Doses (E, in J/cm^2) in "XL-x", Where "-x" Stands for the UV Irradiation Time in minutes (with 1 min Corresponding to Approximately 0.1 J/cm^2)

			φ			
buffer	XL	E [J/cm^2]	25 °C	29 °C	32 °C	38 °C
PBS	XL-5	0.52	0.03	0.03	0.03	0.04[a]
PBS	XL-10	1.04	0.05	0.05	0.05	0.10[a]
PBS	XL-15	1.57	0.09	0.11	0.13	0.18[a]
ACT	XL-5	0.52	0.06	0.07	[b]	[b]
ACT	XL-10	1.04	0.09	0.09	[b]	[b]
ACT	XL-15	1.57	0.15	0.20	[b]	[b]

[a]These values have been acquired by extrapolation of the data from hydrogels at same temperature using an empirical relation with the radiation dose.[28] [b]Because of the very strong hydrogel collapse, the fluorescence signal for tracers in acetate (ACT) buffer was not measurable for temperatures $T > 29$ °C.

concentration in the hydrogel, and (III) temperature effects, which are discussed below.

I. Swelling Ratio. The example in Figure 1 illustrates that the studied hydrogel films swell less in the acetate buffer compared to PBS. The reason is that the pNiPAAm-based terpolymer backbone includes about 5% of ionizable methacrylic acid units, in addition to the 94% of neutral NiPAAm units as the main component, and 1% hydrophobic benzophenone-based cross-linker. The carboxyl groups of the methacrylic acid exhibit a pK_a ∼ 4.5. Incorporation of such monomer into the polymer increases the effective pK_a by about 1 unit.[81−84] Therefore, the polymer network is substantially negatively charged in the PBS (pH = 7.4), whereas in the acetate buffer (pH = 4) it is almost neutral. The negative charge carried by the polymer chains is accompanied by their electrostatic repulsion among polymer chains in the networks, which translates to the increasing swelling ratio at higher pH. It is worth noting that other parameters also affect the swelling of the polymer network,[34] including screening by free ions in the buffer solution, which reduce the effect of electrostatic interactions. However, they have apparently only a minor effect under the present conditions.

II. pH Dependence of Tracer Concentration. Second, the intensity profile of the fluorescence signal $I(z)$ originating from fluorescent tracers present inside the hydrogel layer differs for PBS and acetate buffers, as seen in Figure 1. The higher $I(z)$ values observed in ACT compared to PBS at $T = 25$ °C appear contradictory to the lower swelling ratio R_s in acetate buffer, where a smaller pore volume in the polymer network is expected to hinder permeation of the large IgG molecules. However, this observation can be explained by the pH-dependent electrostatic interaction between the A647-labeled IgG and the carboxylated hydrogel network. The isoelectric point of the native IgG is pI = 8−9. We determined experimentally that this value decreases significantly to pI ∼ 5−6 for the labeled antibody conjugated with A647 fluorophores (Figure S1, Supporting Information). This effect is expected to result from a reduced number of free amino groups on the IgG molecules, which are transformed to neutral amide groups in the labeling reaction. Consequently, in PBS with pH 7.4 the labeled IgG is negatively charged, the same as the hydrogel network with carboxyl groups. Electrostatic repulsions apparently dominate their mutual interactions, as reflected in the lower intensity $I(z)$.

On the contrary, in acetate buffer with pH = 4 the labeled IgG becomes positively charged while the hydrogel network may still carry a weak negative charge. In this case, the electrostatic interactions between the labeled IgG and the hydrogel are slightly attractive, and the fluorescence intensity in the hydrogel is higher than in PBS. However, it is still lower than in the bulk liquid, which cannot be explained by electrostatics anymore. This reduced intensity indicates an additional repulsive interaction, which can be ascribed to the excluded volume of the rather large IgG molecule leading to steric repulsion from the polymer network. The excluded volume contribution becomes more pronounced at higher polymer volume fractions (low pH or high T). We should recall that $I(z)$ originates from both labeled IgG and residual free molecular dye and their contribution to a time-averaged quantity is indistinguishable in the static case probed solely by the fluorescence intensity. Since the free A647 dye bears four strong negatively charged SO_3^- groups,[85] which are insensitive to the different pH in acetate or PBS buffer, its electrostatic interaction with the hydrogel should always be repulsive, thus hindering its penetration into the hydrogel layer. Therefore, the z-scans of Figure 1 predominantly reflect changes in the partitioning of IgG as the average fluorescence intensity being proportional to the tracer concentration in a given phase (c_g in the hydrogel and c_s in the solution). It is worth of noting that the partitioning of the two tracers can be independently discriminated by dynamics measurements as discussed in subsection B. The validation of both methods for determination of IgG partition coefficients can be found in Figure S2. Both partition coefficients and tracer dynamics (subsection B) were calculated at the midpoint of the estimated thickness of each hydrogel, inferred from the z-scan. This experiment protocol excludes position artifacts related to the proximity to the interfaces

III. Temperature Dependence of Partitioning. The dependence of the fluorescence signal profiles $I(z)$ on temperature was investigated for hydrogel layers with varied polymer volume fraction ϕ, controlled by the cross-link density, swollen in PBS and acetate buffer. The respective partition coefficient P of the A647-labeled IgG was determined as the ratio of $I(z)$ inside and outside the hydrogel layer, which well approximates the ratio of IgG concentration c_g/c_s (see Supporting Information Figure S2 and section S2 for additional details). In Figure 2, the partition coefficient P is plotted as a function of ϕ and T, where the data for PBS are indicated by solid symbols and for acetate buffer by open symbols. Each data set for a specific cross-link density (i.e., XL-5, XL-10, and XL-15) is clustered within a color-coded cloud, indicating a temperature increase by the color gradient going from blue to red. Two cases of ϕ variation have to be distinguished: (1) By increasing the irradiation energy dose/time during film preparation, the cross-linking density of the polymer network (and thus ϕ) also increases (from XL-5 to XL-15). (2) By increasing the temperature, the gel becomes more hydrophobic and excludes water, which is accompanied by its collapse (increase in ϕ) above the lower critical solution temperature (LCST, typically around 32 °C in water). For case 1 of increasing cross-link density at low temperature (in the highly swollen state) the P values decrease significantly (going from squares over triangles to circles in Figure 2). As such, tracer partitioning between the aqueous phase and the hydrogel network is dominated by like-charge repulsion at 25 °C in the

DOI: 10.1021/acs.macromol.7b00514
Macromolecules XXXX, XXX, XXX−XXX

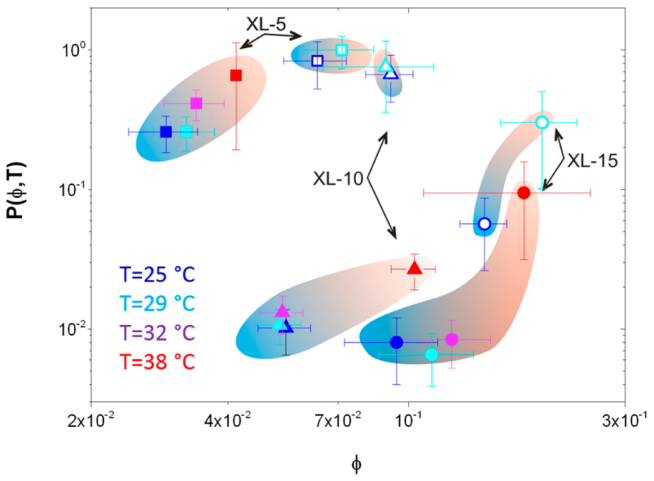

Figure 2. Effective partition coefficient $P(\phi,T)$ of IgG-A647 conjugate as a function of hydrogel volume fraction ϕ and temperature T. Hydrogel layers with varied cross-linking density XL-5 (squares), XL-10 (triangles), and XL-15 (circles) were examined at temperature T = 25 °C (blue), 29 °C (cyan), 32 °C (violet), and 38 °C (red). The $P(\phi,T)$ is shown for the hydrogel layers swollen in PBS (filled symbols) and ACT (open symbols) buffers. For each buffer and cross-link density, the three shaded areas indicate the trend in the variation of P with increasing temperature T.

swollen state in PBS buffer, and by excluded volume in the ACT buffer, supporting the arguments of the preceding paragraph. Thus, for ACT buffer the observed decrease of partitioning coefficient $P(\phi,T)$ with ϕ reflects enhanced crowding effects due to the reduced hydrogel mesh size. Unexpectedly, for case 2 gradual increase in partitioning coefficient $P(\phi,T)$ is observed when increasing temperature below the LCST, and an abrupt increase in P occurs when the gel collapses at temperature above the LCST (color-coded from blue to red in Figure 2). Interestingly, this temperature dependence of the partitioning coefficient $P(\phi,T)$ shows a trend that is opposite to the case 1 as more fluorescent tracers accommodate inside the densified hydrogel with higher ϕ. Such behavior is contradictory to what could be expected from the electrostatic and excluded volume arguments given above (though for XL-5 and XL-10 in acetate buffer it varies only weakly between 25 and 29 °C, within the estimated uncertainty). This tracer accumulation (as apparent from Figure 2, specifically for the red symbols/PBS and cyan symbols/ACT) indicates the presence of an additional attractive tracer−hydrogel interaction particularly at elevated temperature, which could be ascribed to increasing hydrophobicity of the pNiPAAm polymer chains as the temperature approaches and exceeds its LCST of about 32 °C in pure water.

Support for this hypothesis can be found in independent experiments performed with similar pNiPAAm layer systems. For example, the interaction of a hydrophobic AFM tip with the pNiPAAm hydrogel films in water revealed increasing attraction to the polymer network with increasing temperature, below, as well as above the LCST of the polymer ($T \sim 32$ °C).[36] When approaching the LCST, the solvent quality decreases abruptly, which renders the hydrogel more hydrophobic and which is consistent with the temperature-induced collapse of these pNiPAAm hydrogel layers in pure water. The concurrent increase in partitioning P of the tracers with higher temperature in both PBS and acetate buffers is due to the hydrophobicity effect that favors tracer−hydrogel attraction. Proteins, such as IgG, are partially hydrophobic, owing to hydrophobic side chains of the amino acid residues. Consequently, IgG is strongly attracted to hydrophobic surfaces, as demonstrated by IgG adsorption onto hydrophobized nanowires.[85] Consequently, the hydrophobic attraction between IgG and the hydrogel increases with increasing temperature (Figures S2 and S3). Because the hydrogel layers collapse much stronger in acetate buffer compared to PBS (see Table 1), the highly collapsed hydrogel in acetate buffer completely suppresses tracer diffusion inside the polymer network at temperatures around the LCST. Thus, the fluorescence signal for tracers in acetate buffer was not measurable at T > 29 °C, and the corresponding partition coefficients could not be obtained.

In summary, the influence of the three experimental parameters (cross-linking density, temperature and buffer pH) on the hydrogel swelling ϕ, and on IgG partitioning P, can be rationalized by the structural and thermodynamic characteristics of the polymer network (mesh size, charge, hydrophobicity) and by the charge and amphiphilicity of the A47-labeled IgG. The interplay of interactions is illustrated in Table 2 and their influence on the labeled IgG diffusion dynamics is discussed in the next section.

Table 2. Influence of Stimuli on the Properties of Hydrogel and IgG with an Overview of Their Mutual Interaction Mechanisms

	PBS (pH = 7.4)	acetate (pH = 4)	increasing cross-link density	increasing temperature
hydrogel ($pK_a \sim 4.5$)	negative charge	about neutral	decreasing swelling ratio	increasing hydrophobicity
labeled IgG (pI ~ 5.5)	negative charge	positive charge	(not applicable)	no sign. effect
dominant IgG/hydrogel interaction	repulsive	weak attraction	excluded-volume	hydrophobic

B. Protein Diffusion. The attractive interaction between hydrogel and the labeled IgG is expected to affect the translational mobility of this tracer in the pNiPAAm network.[87] This mobility change is investigated by using the normalized FCS autocorrelation function $G(t)$, representative examples of which are shown in Figure 3 at good solvency conditions (25 °C) for two cross-linking densities (XL-5 and XL-15) in PBS buffer (Figure 3a) and acetate buffer (Figure 3b). These $G(t)$ attain a shape qualitatively deviating from a single decay. This character is more pronounced for the highly cross-linked hydrogel XL-15 than for the weakly cross-linked hydrogel XL-5. The measured $G(t)$ can be well represented by two component Fickian diffusion processes (eq 1) that yield two coefficients: D_f for a fast and D_s for a slow diffusion process with amplitudes F_f and F_s, respectively (see Experimental Section). The fast coefficient D_f is ascribed to the diffusion coefficient of the free A647 dye, concomitantly present as residual after the fluorophore labeling process of IgG. The slow diffusion component, described by D_s and the amplitude F_s, is associated with the diffusion of the large A647-labeled IgG. Moreover, the established baseline in $G(t)$ suggests tracer diffusion under ergodic conditions, which is also supported by the robustness of $G(t)$ with respect to variation of the measurement position for the probed spot inside the hydrogels (data not shown).

DOI: 10.1021/acs.macromol.7b00514
Macromolecules XXXX, XXX, XXX−XXX

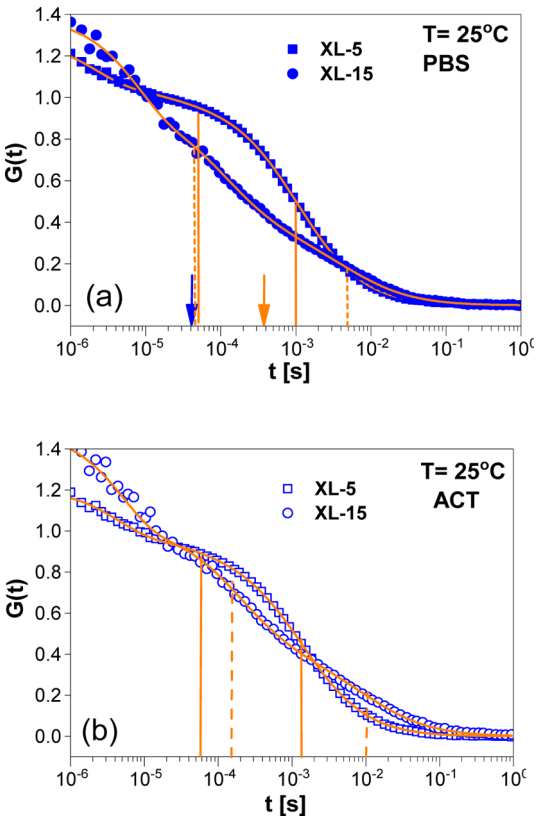

Figure 3. Examples of normalized fluorescent intensity autocorrelation functions $G(t)$ recorded concurrently for A647-labeled IgG and free A647 at 25 °C in hydrogel layers with cross-linking density XL-5 (squares) and XL-15 (triangles) swollen in (a) PBS and (b) ACT buffers. Dashed and solid vertical lines indicate the extracted fast and slow diffusion times by using a double Fickian diffusion representation of the experimental $G(t)$. Blue and orange arrows denote the diffusion time of the free A647 and A647-labeled IgG in buffer outside the hydrogel layer.

This free A647 dye was detectable in the labeled IgG solutions by FCS (Supporting Information, section 4 and Figure S4), while thin layer chromatography (TLC, section S5 and Figure S5) did not provide evidence of such impurity. We note that samples for both techniques were prepared under identical conditions, but FCS has much higher (single molecule detection) sensitivity. It is worth noting that the diffusion of solely A647 (fast component in herein presented experiments) in identically prepared pNiPAAm hydrogel layers was investigated before in water and acetate buffer.[28]According to therein reported observations, A647 alone behaves as a noninteracting tracer, and its diffusion can be analyzed by using one-component representation of $G(t)$. A more complicated two-component fit was necessary only for dense hydrogel films at higher temperatures (in the precollapsed state), in which an additional faster diffusion component appeared.[28] The herein reported work focuses at diffusion of fluorescent tracers through hydrogel layers with higher swelling ratio, and the use of two-component fitting allows to determine the relative contribution of free A647 to A647-labeled IgG as well as to account for stimuli-driven interactions of the labeled IgG with the polymer hydrogel.

In the current work the tracer−gel interactions play a significant role, and we provide direct evidence of their nature by means of partition coefficients. The combination of the thermodynamic information (interactions) from the partition coefficients and of the dynamical information from $G(t)$ is the strength and the added value of the current work. The slow diffusion component and its relative contribution (amplitude) in Figure 3 characterize the dynamics and the population of the large A647-labeled IgG in the complex hydrogel environment, while the presence of the fast component indicates penetration of the small molecular tracer (free A647 dye) inside the polymer network. The relative contribution of the slow component F_s ($F_s = 1 - F_f$ in eq 1) is shown for PBS in the lower panel of Figure 4 and correlates well with the partition

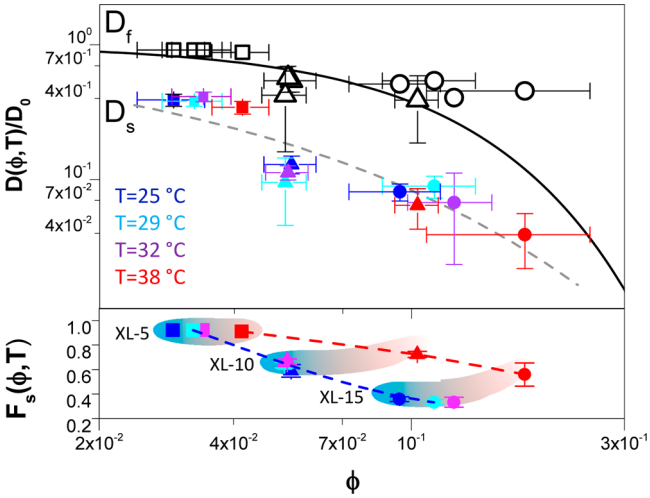

Figure 4. Diffusion slowdown as represented by the normalized diffusion constant $D(\phi,T)/D_0$ (upper panel) and amplitude of the slow component $F_s(\phi)$ (lower panel) as a function of polymer volume fraction ϕ and temperature T in PBS buffer. D_f corresponds to the free A647 dye while the D_s and F_s are attributed to the A647-IgG conjugate. Hydrogel layers with varied cross-linking density XL-5 (squares), XL-10 (triangles), and XL-15 (circles) were examined at temperature T = 25 °C (blue), 29 °C (cyan), 32 °C (violet), and 38 °C (red). The solid black curve denotes the fitted exponential curve corresponding to diffusion slowdown for noninteracting molecular dyes in hydrogels.[28] The dashed gray line in the upper panel is a stretched exponential representation of D_s, while the two dashed lines (red and blue) in the lower panel are drawn to guide the eye.

coefficient P of the larger tracer, as discussed above (Figure 2). Below 32 °C the amplitude F_s is weakly affected by temperature, in contrast with an abrupt amplitude increase at 38 °C (again in agreement with the static approach for P, as discussed in subsection A). Furthermore, the fast diffusion component $D_f(\phi)$ (ascribed to free A647) conforms well to the scaling behavior (solid black curve in the upper panel of Figure 4) reported for molecular diffusion within the polymer network in the absence of specific interactions. This behavior offers the great opportunity to use the free A647 dye as independent reporter tracer that diffuses simultaneously with the large and interacting tracer, A647-labeled IgG, in the same hydrogel environment. In the present section, the main focus lies on the dynamics and the population of the large, labeled IgG antibody inside the pNiPAAm hydrogel layers, which can thus be directly compared to the small tracer behavior under identical experimental conditions.

We define the translational diffusion slowdown as the ratio of the diffusion constant $D(\phi,T)$ in the center of the gel and the corresponding diffusion constant D_0 of the free tracer in pure

DOI: 10.1021/acs.macromol.7b00514
Macromolecules XXXX, XXX, XXX−XXX

solvent. The upper panel of Figure 4 shows the diffusion slowdown of the A647-labeled IgG as a function of the hydrogel volume fraction ϕ for the three different hydrogels (XL-5, XL-10, and XL-15) in PBS at different temperatures: T = 25, 29, 32, and 38 °C. A significant reduction of the mobility of the A647-labeled IgG (solid symbols and dashed line) is observed compared to the free A647 (open symbols, solid line) not only with increasing ϕ but also with increasing temperature T. Albeit the latter should be anticipated due to the increasing $\phi(T)$ and hence decreasing free pore volume in hydrogels, strong tracer−matrix interactions manifested in the T-dependent partition coefficient (see Figure 2) should also impact the dynamics. In PBS, both hydrogels and the labeled IgG tracer are negatively charged, resulting in repulsive electrostatic interactions. With increasing temperature, however, hydrophobic interactions can become dominant as suggested by the abrupt increase of $P(T)$ (see Figure 2 and discussion on the static picture in subsection A). The latter trend is also qualitatively revealed in the relative contribution $F_s(T)$ of the IgG−A647 tracer to the relaxation function $G(t)$ shown in the lower panel of Figure 4. At the highest temperature above the LCST (which is 32 °C in pure water) an abrupt increase of $F_s(T)$ is observed, yet with a significantly smaller magnitude compared to the analogous increase of $P(T)$. Such an up-turn behavior is absent in the IgG−A647 translational diffusion represented by $D_s(\phi,T)$.

However, based on the systematic deviation of D_s from the D_f trend (for A647) in the composition dependence (solid black line in the upper panel of Figure 4) with increasing temperature for XL-5 (with the lowest cross-link density), crowding alone (as was for A647 in earlier work) is not a sufficient mechanism to account for the complex behavior of the measured IgG tracer diffusion. Together with D_s, we also used D_f and performed the fitting in two ways: with D_f as floating parameter or fixed to the values previously reported for A647 in similar hydrogels.[28] The values of D_s, obtained by the two procedures, did not differ by more than 10%. Therefore, we concluded that both D_f and D_s are robust, and D_f is consistent with the master curve for the free dye.

In the absence of interactions, the slowdown $D_s(\phi)/D_0$ is controlled by the confinement and crowding effects determined by the tracer size (hydrodynamic radius R_h = 6.5 nm for the A647-labeled IgG, see Experimental Section and also Supporting Information, section S4), mesh size ($\xi[\phi]$) of the network and corresponding free pore volume, and the polymer concentration.[88−90] It is usually captured by a semiempirical stretched exponential fit, $D = D_0 \exp(-A\phi^{\alpha})$. By fitting the measured data $D_s(\phi)/D_0$, the parameters A = 9.5 and α = 0.55 were determined (see dashed gray line in upper panel of Figure 4). The values of these parameters are significantly smaller than the corresponding values (A = 20.5 and α = 1.35) determined for free A647 dye (solid black line in the upper panel of Figure 4). It is worth noting that the latter values are consistent with those measured before for free A647 diffusion in analogous hydrogels.[28]

On the other hand, the observation of a single IgG diffusion even at the highest examined temperature, where attraction is anticipated from the increase of $P(T)$ and $F_s(T)$, precludes an unambiguous identification of the specific enthalpic interactions. Only the presence of a two component diffusion of the IgG tracer, free and bound to the pNiPAAm segments, could allow an estimation of the attractive hydrophobic interactions.[87] Hence, we assume that the experimental $D_s(\phi,T)$ represents an effective, averaged diffusion of the IgG tracer with strong temperature-induced slowdown with increasing ϕ (decreasing $\xi(\phi)$ and free pore volume), as seen for the higher cross-linking density hydrogels (XL-10 and XL-15 in Figure 4). The temperature effect on $D_s(\phi,T)$ is captured in the $\phi(T)$, including interactions as discussed in the preceding sections.

The increasing $P(T)$ and $F_s(T)$ at temperatures below the LCST is a clear evidence of strong attractive interactions, which should influence the large tracer dynamics. In fact, two diffusive processes have been reported for a molecular dye ($R_h \sim 0.6$ nm) in pNiPAAm solutions in the presence of attractive interactions[87] assigned to diffusion of a free tracer (D_{free}) and to diffusion of a tracer bound to the polymer chain (D_{bound}). In an FCS experiment, a particular process can be resolved only if the characteristic diffusion length, associated with the free or bound state (L_{bound} and L_{free}), is larger than the focal spot size w (~300 nm). At the same time, numerical stability of the fitting procedure allows the resolution of two processes only if $D_{free}/D_{bound} > 5$. In the opposite case, if the switching dynamics is too fast, the fluorophore repeatedly changes its state while traveling over the focal volume, and one observes an effective single-component diffusion. Over the bound time, $t_{bound} \approx \exp(U/kT)$, the displacement length $L_{bound} \approx (D_{bound}t_{bound})^{1/2}$ sensitively depends on the binding energy U. The observation of a single slow diffusion (Figure 3) suggests that the consequence of the two distinct mechanisms are averaged out before the A647-labeled IgG leaves the focal spot ($L_{bound} < w$), yielding an effective $D_s(\phi,T) = D_{bound}f + D_{free}(1-f)$, where f is the fraction of the bound tracers. At 38 °C, the A647-labeled IgG in XL-15 diffuses about 25 times slower than in free PBS buffer ($(3.5 \pm 0.2) \times 10^{-11}$ m^2 s^{-1}), implying an upper value for $t_{bound} < 10$ ms. While it is not experimentally easy to reduce w, increase of the attractive hydrophobic interactions with temperature should increase t_{bound} and hence fulfill the resolution condition, $L_{bound} > w$, provided that D_{bound} remains virtually constant. We discuss this notion in the next paragraph for the same hydrogel/tracer system in acetate buffer.

The repulsive electrostatic interaction between the A647-labeled IgG and the hydrogel in PBS buffer turns to attractive in acetate buffer due to the reversal of the protein charge, which impacts the tracer penetration (Figure 2). Concurrently, the negative charge of the hydrogel chains in PBS is reduced in acetate buffer, thereby allowing hydrophobic attractions to gain a more significant role. Note the larger values in $\phi(T)$ at the same T, as well as the absolute changes in $\phi(T)$, for acetate buffer compared to PBS buffer (Table 1) due to stronger hydrophobic attractions in acetate buffer. The IgG tracer diffusion characteristics (slowdown and F_s) displayed in Figure 5 for acetate buffer are qualitatively similar to those in PBS. However, the trend is generally enhanced in acetate buffer as compared to PBS at identical temperatures. For high temperatures, the system in acetate buffer becomes nonergodic in the FCS time window, thus precluding the measurement of fully relaxed $G(t)$ above 29 °C in acetate (see Figure S3). At lower temperatures T = 25 and 29 °C, the experimental function $G(t)$ is robust with respect to the change of the IgG−hydrogel interactions in acetate buffer, since it can still be represented by a single slow process with an effective $D_s(\phi,T)$. However, inspection of the $D_s(\phi,T)$ in Figure 5 reveals the failure of data superposition, which was less apparent in the data of Figure 4. In acetate buffer, the tracer diffusivity abruptly drops above $\phi \sim 0.1$. Since slowdown of the slow component is (i) stronger than for A647 (ref 28) and (ii) comparable in the

DOI: 10.1021/acs.macromol.7b00514
Macromolecules XXXX, XXX, XXX−XXX

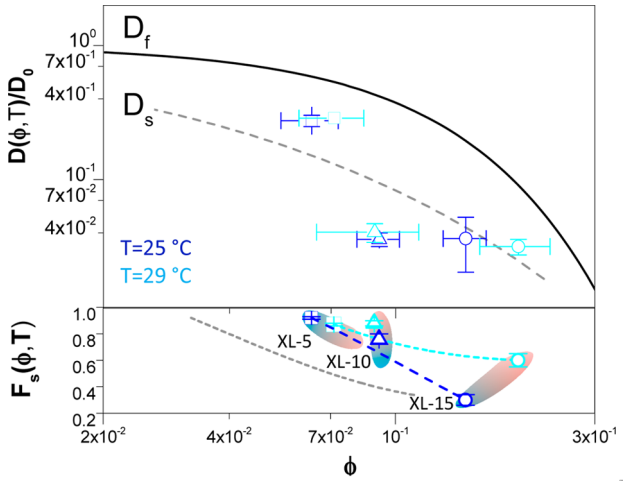

Figure 5. Diffusion slowdown $D(\phi,T)/D_0$ (upper panel) and amplitude of the slow component $F_s(\phi)$ (lower panel) as a function of polymer volume fraction ϕ and temperature T in ACT buffer. Hydrogel layers with varied cross-linking density XL-5 (squares), XL-10 (triangles), and XL-15 (circles) were examined at temperature 25 °C (blue) and 29 °C (cyan). The solid black curve in the upper panel denotes the diffusion slowdown for noninteracting molecular dyes in hydrogels.[28] The dashed gray line in the upper panel is the stretched exponential representation of D_s, while the blue and cyan dashed lines in the lower panel are drawn to guide the eye. The dashed gray line in the lower panel denotes the fit through data from the analogous panel in PBS at good solvency.

two buffers at the same volume fraction in identical pNiPAAm hydrogels, its behavior cannot originate from A647 and clearly represents the diffusion of IgG in the gels. The decrease of the slow component fraction with increasing cross-link density is rather a "filtration" effect, progressively ruling out penetration of the larger IgG and thus decreasing its concentration in the gels. Utilizing arguments from photophysics and dynamics, our presented work provides a systematic methodology that rules out relations of the observed slowdown to the molecular dye itself but rather hints to the transport of the labeled antibody.

Concluding Remarks. Our experiments have shown that the diffusion slowdown of fluorescently labeled IgG tracer in dual thermo- and pH-responsive polymer hydrogels is a robust function of polymer volume fraction. This observation is in strong contrast with the complex partitioning behavior of IgG between the swollen hydrogel matrix and the bulk solution, being influenced by a complex interplay of three interactions. Each interaction dominates the overall behavior under certain conditions. Electrostatic repulsion dominates both hydrogel swelling and IgG partitioning in PBS buffer (pH = 7.4), where both the hydrogel ($pK_a \sim 4.5$) and IgG (pI ~ 5) are negatively charged, while it is negligible in acetate buffer (pH = 4) where both are nearly neutral to slightly positive. The effect of excluded volume is significant especially at high hydrogel volume fractions (low swelling) induced by lower pH, higher temperature, or extended cross-linking. Last but not least, the hydrophobic interaction gains relevance at higher temperature (specifically above the LCST) and high cross-link densities. The overall effect of IgG–hydrogel interactions as a sum of the above contributions leads to a complex dependence of partitioning on hydrogel volume fractions, which could not be explained if any of the above contributions is neglected. The static picture of the fluorescence intensity profiles provides information about the location of the interface between the hydrogel and aqueous solution, concerning the hydrogel swelling ratio, and about the thermodynamics of IgG–hydrogel interactions from tracer partitioning. Monitoring of the diffusion dynamics via FCS allows us to separate the fast mode of the free dye from the slow mode of the labeled IgG tracer. Only after this separation it is possible to extract the diffusion coefficient of IgG inside the hydrogel environment. By accounting for the amplitudes of the slow and fast contributions to $G(t)$, it is possible to unambiguously determine partition coefficients for IgG. Consistency of the data from this dynamics determination with the static values of partition coefficient P obtained from the z-scans a posteriori justifies our interpretation. It demonstrates the synergistic role of static and dynamic properties in providing relevant information about both thermodynamics and diffusion. This determination also demonstrates the power of FCS for in situ studies of diffusion processes of complex molecules interacting with multi-responsive environments, where the host environment and the guest tracer both respond to external stimuli and influence each other in a nontrivial way.

EXPERIMENTAL SECTION

Solvent and Polymer Specifications. The following solvents were used: 10 mM phosphate buffered saline, PBS (140 mM NaCl, 10 mM phosphate, and 3 mM KCl, pH adjusted to 7.4 at 25 °C) from Calbiochem and acetate buffer (10 mM sodium acetate and acetic acid mixture 1:1, pH adjusted to 4 by means of HCl and NaOH). The random terpolymer of pNiPAAm (94 mol % NiPAAm; 5% methacrylic acid; 1% benzophenone methacrylate cross-linker) was synthesized by free radical polymerization.[80] The weight-averaged molecular mass of the polymer and its dispersity amount to M_w = 280K and $Đ$ = 2.7, respectively. The overlap concentration in water is c^* ~ 0.003 g/mL. The grafting agent 4-(3-triethoxysilyl)propoxybenzophenone ("benzophenone silane") was synthesized according to the literature[33] by hydrosilylation of 4-allyloxybenzophenone.

Sample Preparation. A round microscope cover glass was prefunctionalized with ethanolic solution of benzophenone–silane overnight under argon atmosphere and ambient temperature, followed by 1 h warming at T = 50 °C for 1 h, before copiously rinsing of the slides by excess ethanol. Ethanolic solution with dissolved pNiPAAm polymer at a concentration of 10 wt % was spin coated at room temperature onto the prefunctionalized round microscope cover glass slides. The thickness of the layer was controlled by the rotation speed and 250 rpm was applied for 60 s. After the deposition of pNiPAAm-based layer, the slides were annealed in vacuum for 1 h at a temperature (T = 170 °C) higher than the polymer's glass transition temperature, in order to relieve the polymer system from possible stresses and to remove the solvent. The slides were subsequently dried overnight at T = 50 °C in a vacuum. Afterward, the polymer was cross-linked by UV irradiation (Stratalinker 2400, Stratagene) at λ = 365 nm for the time between 5 and 15 min (60 min of cross-linking corresponds to an irradiation energy dose of 6.28 J/cm^2). Before measuring their dry thickness by using a Stylus profilometer (KLA-Tencor), the cross-linked layers were subsequently rinsed with copious amounts of ethanol and fully dried under gas nitrogen atmosphere.

Tracer. The A647-labeled IgG was obtained from Life Technologies (A-21235, now Thermo Fischer Scientific). The number of ~5 bound A647 dyes per IgG was estimated from FCS experiments (section S4) as the ratio of molecular fluorescence brightness of the A647- labeled IgG relative to that of free Alexa 647 (from Thermo Fischer Scientific) determined under the same experimental conditions. The hydrodynamic radius of the A647-labeled IgG (R_h = 6.5 nm) was measured in water by FCS (see also section S4), which agrees with values reported for unlabeled IgG (5–6 nm).[91] The hydrodynamic radius of the A647 tracer R_H = 0.74 nm is known from the literature.[92] Interestingly, a residual free A647 was detectable by FCS in all used samples with A647-labeled IgG, while thin layer

DOI: 10.1021/acs.macromol.7b00514
Macromolecules XXXX, XXX, XXX–XXX

chromatography showed no free A647 dye in the A647-labeled IgG sample. It is worth of noting that the presented experiments took advantage of this as A647 is commonly used as a reference dye for calibration of the FCS focal spot. Its translational diffusion coefficient can be measured independently as it is about order of magnitude faster than that of A647-labeled IgG. The isoelectric point of the labeled IgG was determined by isoelectric focusing (IEF) with pH gradient polyacrylamide gel electrophoresis (see section S1).

FCS Experiments and Analysis. The experiments were performed using an inverted confocal microscope Axiovert 200 from Carl Zeiss (Jena, Germany) with the Confocor2 module for FCS analysis. A 40× high numerical aperture (NA = 1.2) C-Apochromat 40×/1.2 W water immersion objective with working distance of 280 μm was used. A HeNe laser at λ = 633 nm was used to excite A647-labeled IgG (and the free dye A647). The same objective was used to collect the fluorescent light, which, following passage through a LP650 emission filter and a confocal pinhole, arrived at an avalanche photodiode detector capable of single-photon counting. The diffusion of fluorescent tracers through the focal spot caused temporal fluctuations of the detected fluorescence intensity, $\delta I(t)$. These fluctuations were recorded and evaluated by the software correlator in terms of an autocorrelation function $G(t) = 1 + \langle \delta I(t')\delta I(t' + t)\rangle / \langle I(t')\rangle^2$. Everywhere in this work, the double Fickian diffusion formula (eq 1) was used to fit the $G(t)$ curves of IgG: in the hydrogels, in the reference IgG measurements of dilute pNiPAAm solutions in acetate and PBS buffer as well as in the absence ofpNiPAAm (blank samples with solely buffers):[93]

$$G'(t) = 1 + \frac{1}{N}\left(1 + \frac{T'}{1 - T'}e^{-t/\tau_T}\right)\sum_{i=1}^{n} \frac{F_i}{\left(1 + \frac{t}{\tau_i}\right)\sqrt{\left(1 + \frac{t}{S^2\tau_i}\right)}} \quad (1)$$

T' and τ_T are the fraction and the decay time of the triplet state. N is the average number of fluorescent species in the FCS probing volume, and F_i and τ_i represent the amplitude fraction and the lateral diffusion time through the FCS focal spot, of species i, with $D_i = w_0^2/4\tau_i$ the respective diffusion coefficient. Next, $S = w_0/z_0$ is the so-called structural parameter giving the ratio between the axial ($2z_0$) and the lateral ($2w_0$) dimensions of the FCS focal spot. The selected formula accounts for two diffusing populations ($n = 2$), simultaneously crossing the FCS focal spot: a fast one (free dye, A647) and a slower one (A647-labeled IgG).

■ ASSOCIATED CONTENT

Supporting Information

The Supporting Information is available free of charge on the ACS Publications website at DOI: 10.1021/acs.macromol.7b00514.

Isoelectric point (pI) determination of unlabeled IgG and fluorophore Alexa Fluor 647-labeled IgG, determination of the partition coefficient $P(\phi,T)$ for IgG, $G(t)$ vs t dynamics of IgG close to the LCST/acetate buffer, determination of the size and degree of labeling of the IgG, thin layer chromatography (TLC) analysis of A647-labeled IgG tracer versus free A647 dye (PDF)

■ AUTHOR INFORMATION

Corresponding Author

*E-mail: fytas@mpip-mainz.mpg.de (G.F.).

ORCID

J. Dostalek: 0000-0002-0431-2170

Notes

The authors declare no competing financial interest.

■ ACKNOWLEDGMENTS

This work was financially supported by the Deutsche Forschungsgemeinschaft, in the framework of SPP1259 "Intelligence Hydrogele", SPP 1066. G.F. thanks AIT for the hospitality, and P.K. acknowledges support from the Czech Science Foundation, Grant No. 17-02411Y. Technical support from Katja Nilles for the synthesis of the pNiPAAm polymer is gratefully acknowledged.

■ REFERENCES

(1) Lee, B. P.; Konst, S. Novel Hydrogel Actuator Inspired by Reversible Mussel Adhesive Protein Chemistry. *Adv. Mater.* **2014**, *26* (21), 3415−3419.

(2) Morales, D.; Palleau, E.; Dickey, M. D.; Velev, O. D. Electro-actuated hydrogel walkers with dual responsive legs. *Soft Matter* **2014**, *10* (9), 1337−1348.

(3) Yuk, H.; Zhang, T.; Lin, S.; Parada, G. A.; Zhao, X. Tough bonding of hydrogels to diverse non-porous surfaces. *Nat. Mater.* **2015**, *15* (2), 190−196.

(4) Hu, Y.; Lu, C.-H.; Guo, W.; Aleman-Garcia, M. A.; Ren, J.; Willner, I. A Shape Memory Acrylamide/DNA Hydrogel Exhibiting Switchable Dual pH-Responsiveness. *Adv. Funct. Mater.* **2015**, *25* (44), 6867−6874.

(5) Han, L.; Lu, X.; Wang, M.; Gan, D.; Deng, W.; Wang, K.; Fang, L.; Liu, K.; Chan, C. W.; Tang, Y.; Weng, L.-T.; Yuan, H. A Mussel-Inspired Conductive, Self-Adhesive, and Self-Healable Tough Hydrogel as Cell Stimulators and Implantable Bioelectronics. *Small* **2017**, *13*, 1601916.

(6) Fang, Y.; Wang, C.-F.; Zhang, Z.-H.; Shao, H.; Chen, S. Robust Self-Healing Hydrogels Assisted by Cross-Linked Nanofiber Networks. *Sci. Rep.* **2013**, *3*, 2811.

(7) Wang, Q.; Gao, Z. A constitutive model of nanocomposite hydrogels with nanoparticle crosslinkers. *J. Mech. Phys. Solids* **2016**, *94*, 127−147.

(8) Chen, F.; Yu, S.; Liu, B.; Ni, Y.; Yu, C.; Su, Y.; Zhu, X.; Yu, X.; Zhou, Y.; Yan, D. An Injectable Enzymatically Crosslinked Carboxymethylated Pullulan/Chondroitin Sulfate Hydrogel for Cartilage Tissue Engineering. *Sci. Rep.* **2016**, *6*, 20014.

(9) Billiet, T.; Vandenhaute, M.; Schelfhout, J.; Van Vlierberghe, S.; Dubruel, P. A review of trends and limitations in hydrogel-rapid prototyping for tissue engineering. *Biomaterials* **2012**, *33* (26), 6020−6041.

(10) Li, J.; Mooney, D. J. Designing hydrogels for controlled drug delivery. *Nature Reviews Materials* **2016**, *1*, 16071.

(11) Magin, C. M.; Neale, D. B.; Drinker, M. C.; Willenberg, B. J.; Reddy, S. T.; La Perle, K. M. D.; Schultz, G. S.; Brennan, A. B. Evaluation of a bilayered, micropatterned hydrogel dressing for full-thickness wound healing. *Exp. Biol. Med.* **2016**, *241* (9), 986−995.

(12) Sun, G.; Zhang, X.; Shen, Y.-I.; Sebastian, R.; Dickinson, L. E.; Fox-Talbot, K.; Reinblatt, M.; Steenbergen, C.; Harmon, J. W.; Gerecht, S. Dextran hydrogel scaffolds enhance angiogenic responses and promote complete skin regeneration during burn wound healing. *Proc. Natl. Acad. Sci. U. S. A.* **2011**, *108* (52), 20976−20981.

(13) Puchberger-Enengl, D.; Krutzler, C.; Keplinger, F.; Vellekoop, M. J. Single-step design of hydrogel-based microfluidic assays for rapid diagnostics. *Lab Chip* **2014**, *14* (2), 378−383.

(14) Vaisocherova, H.; Yang, W.; Zhang, Z.; Cao, Z. Q.; Cheng, G.; Piliarik, M.; Homola, J.; Jiang, S. Y. Ultralow fouling and functionalizable surface chemistry based on a zwitterionic polymer enabling sensitive and specific protein detection in undiluted blood plasma. *Anal. Chem.* **2008**, *80* (20), 7894−7901.

(15) Wang, Y.; Brunsen, A.; Jonas, U.; Dostalek, J.; Knoll, W. Prostate specific antigen biosensor based on long range surface plasmon-enhanced fluorescence spectroscopy and dextran hydrogel binding matrix. *Anal. Chem.* **2009**, *81* (23), 9625−9632.

(16) Mi, L.; Xue, H.; Li, Y.; Jiang, S. A Thermoresponsive Antimicrobial Wound Dressing Hydrogel Based on a Cationic Betaine Ester. *Adv. Funct. Mater.* **2011**, *21* (21), 4028−4034.

DOI: 10.1021/acs.macromol.7b00514
Macromolecules XXXX, XXX, XXX−XXX

(17) Xu, B.; Li, Y.; Gao, F.; Zhai, X.; Sun, M.; Lu, W.; Cao, Z.; Liu, W. High Strength Multifunctional Multiwalled Hydrogel Tubes: Ion-Triggered Shape Memory, Antibacterial, and Anti-inflammatory Efficacies. *ACS Appl. Mater. Interfaces* **2015**, *7* (30), 16865−16872.
(18) Skardal, A.; Murphy, S. V.; Crowell, K.; Mack, D.; Atala, A.; Soker, S., A Tunable Hydrogel System for Long-Term Release of Cell-Secreted Cytokines and Bioprinted In Situ Wound Cell Delivery. *J. Biomed. Mater. Res., Part B* **2016**, DOI 10.1002/jbm.b.33736.
(19) Lee, D.; Cho, S.; Park, H. S.; Kwon, I. Ocular Drug Delivery through pHEMA-Hydrogel Contact Lenses Co-Loaded with Lipophilic Vitamins. *Sci. Rep.* **2016**, *6*, 34194.
(20) Sharma, N.; Petri, C.; Jonas, U.; Bach, M.; Tovar, G.; Mrkvova, K.; Vala, M.; Homola, J.; Knoll, W.; Dostalek, J. Molecular imprinted polymer waveguides for direct optical detection of small molecules. *Macromol. Chem. Phys.* **2014**, *215* (23), 2295−2304.
(21) Tokuda, T.; Takahashi, M.; Uejima, K.; Masuda, K.; Kawamura, T.; Ohta, Y.; Motoyama, M.; Noda, T.; Sasagawa, K.; Okitsu, T.; Takeuchi, S.; Ohta, J. CMOS image sensor-based implantable glucose sensor using glucose-responsive fluorescent hydrogel. *Biomed. Opt. Express* **2014**, *5* (11), 3859−3870.
(22) Mateescu, A.; Wang, Y.; Dostalek, J.; Jonas, U. Thin hydrogel films for optical biosensor applications. *Membranes* **2012**, *2* (1), 40−69.
(23) Yetisen, A. K.; Butt, H.; Volpatti, L. R.; Pavlichenko, I.; Humar, M.; Kwok, S. J. J.; Koo, H.; Kim, K. S.; Naydenova, I.; Khademhosseini, A.; Hahn, S. K.; Yun, S. H. Photonic hydrogel sensors. *Biotechnol. Adv.* **2016**, *34* (3), 250−271.
(24) Wang, Y.; Huang, C.-J.; Jonas, U.; Wei, T.; Dostalek, J.; Knoll, W. Biosensor based on hydrogel optical waveguide spectroscopy. *Biosens. Bioelectron.* **2010**, *25* (7), 1663−1668.
(25) Huang, C. J.; Dostalek, J.; Knoll, W. Long range surface plasmon and hydrogel optical waveguide field-enhanced fluorescence biosensor with 3D hydrogel binding matrix: On the role of diffusion mass transfer. *Biosens. Bioelectron.* **2010**, *26* (4), 1425−1431.
(26) Lin, C.-C.; Metters, A. T. Hydrogels in controlled release formulations: Network design and mathematical modeling. *Adv. Drug Delivery Rev.* **2006**, *58* (12−13), 1379−1408.
(27) Zustiak, S. P.; Leach, J. B. Characterization of Protein Release from Hydrolytically Degradable Poly(ethylene glycol) Hydrogels. *Biotechnol. Bioeng.* **2011**, *108* (1), 197−206.
(28) Raccis, R.; Roskamp, R.; Hopp, I.; Menges, B.; Koynov, K.; Jonas, U.; Knoll, W.; Butt, H. J.; Fytas, G. Probing mobility and structural inhomogeneities in grafted hydrogel films by fluorescence correlation spectroscopy. *Soft Matter* **2011**, *7* (15), 7042−7053.
(29) Vagias, A.; Košovan, P.; Holm, C.; Butt, H.-J.; Koynov, K.; Fytas, G. Tracer Mobility in Aqueous Poly(N-isopropylacrylamide) Grafted Networks: Effect of Interactions and Permanent Crosslinks. In *Intelligent Hydrogels*; Sadowski, G., Richtering, W., Eds.; Springer International Publishing: 2013; pp 53−62.
(30) Koutsopoulos, S.; Unsworth, L. D.; Nagai, Y.; Zhang, S. Controlled release of functional proteins through designer self-assembling peptide nanofiber hydrogel scaffold. *Proc. Natl. Acad. Sci. U. S. A.* **2009**, *106* (12), 4623−4628.
(31) Gianneli, M.; Beines, P. W.; Roskamp, R. F.; Koynov, K.; Fytas, G.; Knoll, W. Local and Global Dynamics of Transient Polymer Networks and Swollen Gels Anchored on Solid Surfaces. *J. Phys. Chem. C* **2007**, *111* (35), 13205−13211.
(32) Michelman-Ribeiro, A.; Boukari, H.; Nossal, R.; Horkay, F. Structural Changes in Polymer Gels Probed by Fluorescence Correlation Spectroscopy. *Macromolecules* **2004**, *37* (26), 10212−10214.
(33) Modesti, G.; Zimmermann, B.; Börsch, M.; Herrmann, A.; Saalwächter, K. Diffusion in Model Networks as Studied by NMR and Fluorescence Correlation Spectroscopy. *Macromolecules* **2009**, *42* (13), 4681−4689.
(34) Gianneli, M.; Anac, I.; Rostkamp, R.; Menges, B.; Loppinet, B.; Jonas, U.; Knoll, W.; Fytas, G. Dynamic Response of Anchored Poly(N-isopropylacrylamide-co-methacrylic acid-co-benzophenone methacrylate) Terpolymer Hydrogel Layers to Physicochemical Stimuli. *Macromol. Chem. Phys.* **2015**, *216* (3), 277−286.
(35) Gianneli, M.; Roskamp, R. F.; Jonas, U.; Loppinet, B.; Fytas, G.; Knoll, W. Dynamics of swollen gel layers anchored to solid surfaces. *Soft Matter* **2008**, *4* (7), 1443−1447.
(36) Junk, M. J. N.; Berger, R.; Jonas, U. Atomic Force Spectroscopy of Thermoresponsive Photo-Cross-Linked Hydrogel Films. *Langmuir* **2010**, *26* (10), 7262−7269.
(37) Jiang, Z.; Qin, Y.; Peng, Z.; Chen, S.; Chen, S.; Deng, C.; Xiang, J. The simultaneous detection of free and total prostate antigen in serum samples with high sensitivity and specificity by using the dual-channel surface plasmon resonance. *Biosens. Bioelectron.* **2014**, *62*, 268−273.
(38) Zhang, Q.; Jing, L.; Zhang, J.; Ren, Y.; Wang, Y.; Wang, Y.; Wei, T.; Liedberg, B. Surface plasmon resonance sensor for femtomolar detection of testosterone with water-compatible macroporous molecularly imprinted film. *Anal. Biochem.* **2014**, *463*, 7−14.
(39) Wu, A. M.; Senter, P. D. Arming antibodies: prospects and challenges for immunoconjugates. *Nat. Biotechnol.* **2005**, *23* (9), 1137−1146.
(40) Minamiki, T.; Minami, T.; Kurita, R.; Niwa, O.; Wakida, S.-i.; Fukuda, K.; Kumaki, D.; Tokito, S. A Label-Free Immunosensor for IgG Based on an Extended-Gate Type Organic Field Effect Transistor. *Materials* **2014**, *7* (9), 6843.
(41) Kapil, M. A.; Herr, A. E. Binding Kinetic Rates Measured via Electrophoretic Band Crossing in a Pseudohomogeneous Format. *Anal. Chem.* **2014**, *86* (5), 2601−2609.
(42) Schmidt, M. M.; Wittrup, K. D. A modeling analysis of the effects of molecular size and binding affinity on tumor targeting. *Mol. Cancer Ther.* **2009**, *8* (10), 2861−2871.
(43) Moulton, S. E.; Barisci, J. N.; Bath, A.; Stella, R.; Wallace, G. G. Investigation of Ig.G Adsorption and the Effect on Electrochemical Responses at Titanium Dioxide Electrode. *Langmuir* **2005**, *21* (1), 316−322.
(44) Engström, H. A.; Andersson, P. O.; Ohlson, S. Analysis of the specificity and thermodynamics of the interaction between low affinity antibodies and carbohydrate antigens using fluorescence spectroscopy. *J. Immunol. Methods* **2005**, *297* (1−2), 203−211.
(45) Kikuchi, Y.; Uno, S.; Nanami, M.; Yoshimura, Y.; Iida, S.-i.; Fukushima, N.; Tsuchiya, M. Determination of concentration and binding affinity of antibody fragments by use of surface plasmon resonance. *J. Biosci. Bioeng.* **2005**, *100* (3), 311−317.
(46) Roos, H.; Karlsson, R.; Nilshans, H.; Persson, A. Thermodynamic analysis of protein interactions with biosensor technology. *J. Mol. Recognit.* **1998**, *11* (1−6), 204−210.
(47) Liu, T.; Lin, D.-Q.; Zhang, Q.-L.; Yao, S.-J. Characterization of immunoglobulin adsorption on dextran-grafted hydrophobic charge-induction resins: Cross-effects of ligand density and pH/salt concentration. *Journal of Chromatography A* **2015**, *1396*, 45−53.
(48) Zheng, X.; Li, Z.; Beeram, S.; Podariu, M.; Matsuda, R.; Pfaunmiller, E. L.; Ii, C. J. W.; Carter, N.; Hage, D. S. Analysis of biomolecular interactions using affinity microcolumns: A review. *J. Chromatogr. B: Anal. Technol. Biomed. Life Sci.* **2014**, *968*, 49−63.
(49) Du, K. Peptide immobilized monolith containing tentacle-type functionalized polymer chains for high-capacity binding of immunoglobulin G. *Journal of Chromatography A* **2014**, *1374*, 164−170.
(50) Bergström, M.; Åström, E.; Påhlsson, P.; Ohlson, S. Elucidating the selectivity of recombinant forms of Aleuria aurantia lectin using weak affinity chromatography. *J. Chromatogr. B: Anal. Technol. Biomed. Life Sci.* **2012**, *885−886*, 66−72.
(51) Duong-Thi, M.-D.; Bergström, G.; Mandenius, C.-F.; Bergström, M.; Fex, T.; Ohlson, S. Comparison of weak affinity chromatography and surface plasmon resonance in determining affinity of small molecules. *Anal. Biochem.* **2014**, *461*, 57−59.
(52) Handlogten, M. W.; Kiziltepe, T.; Serezani, A. P.; Kaplan, M. H.; Bilgicer, B. Inhibition of weak-affinity epitope-IgE interactions prevents mast cell degranulation. *Nat. Chem. Biol.* **2013**, *9* (12), 789−795.

DOI: 10.1021/acs.macromol.7b00514
Macromolecules XXXX, XXX, XXX−XXX

(53) Bobrovnik, S. A.; Demchenko, M.; Komisarenko, S.; Stevens, F. Traditional ELISA methods for antibody affinity determination fail to reveal the presence of low affinity antibodies in antisera: an alternative approach. *J. Mol. Recognit.* **2010**, *23* (5), 448−456.
(54) Kerr, J. S.; Wright, G. J. Avidity-based Extracellular Interaction Screening (AVEXIS) for the Scalable Detection of Low-affinity Extracellular Receptor-Ligand Interactions. *J. Visualized Exp.* **2012**, No. 61, 3881.
(55) Duong-Thi, M.-D.; Meiby, E.; Bergström, M.; Fex, T.; Isaksson, R.; Ohlson, S. Weak affinity chromatography as a new approach for fragment screening in drug discovery. *Anal. Biochem.* **2011**, *414* (1), 138−146.
(56) Zehn, D.; Lee, S. Y.; Bevan, M. J. Complete but curtailed T-cell response to very low-affinity antigen. *Nature* **2009**, *458* (7235), 211−214.
(57) Moser, A. C.; Hage, D. S. Immunoaffinity chromatography: an introduction to applications and recent developments. *Bioanalysis* **2010**, *2* (4), 769−790.
(58) Ohlson, S. Designing transient binding drugs: A new concept for drug discovery. *Drug Discovery Today* **2008**, *13* (9−10), 433−439.
(59) Mandenius, C.-F.; Wang, R.; Aldén, A.; Bergström, G.; Thébault, S.; Lutsch, C.; Ohlson, S. Monitoring of influenza virus hemagglutinin in process samples using weak affinity ligands and surface plasmon resonance. *Anal. Chim. Acta* **2008**, *623* (1), 66−75.
(60) Winzor, D. J.; Jackson, C. M. Interpretation of the temperature dependence of equilibrium and rate constants. *J. Mol. Recognit.* **2006**, *19* (5), 389−407.
(61) Ohlson, S.; Shoravi, S.; Fex, T.; Isaksson, R. Screening for transient biological interactions as applied to albumin ligands: A new concept for drug discovery. *Anal. Biochem.* **2006**, *359* (1), 120−123.
(62) Butlin, N. G.; Meares, C. F. Antibodies with Infinite Affinity: Origins and Applications. *Acc. Chem. Res.* **2006**, *39* (10), 780−787.
(63) Wiwanitkit, V. Weak binding affinity of immunoglobin G, an explanation for the immune mimicking theory in pathophysiologic findings in the recovery phase of dengue. *Nanomedicine* **2005**, *1* (3), 239−240.
(64) Engberg, K.; Frank, C. W. Protein diffusion in photopolymerized poly(ethylene glycol) hydrogel networks. *Biomed. Mater.* **2011**, *6* (5), 055006.
(65) Markowitz, M. A.; Turner, D. C.; Martin, B. D.; Gaber, B. P. Diffusion and transfer of antibody proteins from a sugar-based hydrogel. *Appl. Biochem. Biotechnol.* **1997**, *68* (1), 57−68.
(66) Reitan, N. K.; Juthajan, A.; Lindmo, T.; de Lange Davies, C. Macromolecular diffusion in the extracellular matrix measured by fluorescence correlation spectroscopy. *J. Biomed. Opt.* **2008**, *13* (5), 054040−054040−9.
(67) Saltzman, W. M.; Radomsky, M. L.; Whaley, K. J.; Cone, R. A. Antibody diffusion in human cervical mucus. *Biophys. J.* **1994**, *66* (2), 508−515.
(68) Chevalier, P.; Cosentino, G. P.; de la Noüe, J.; Rakhit, S. Comparative study on the diffusion of an IgG from various hydrogel beads. *Biotechnol. Technol.* **1987**, *1* (3), 201−206.
(69) Svedhem, Å.; Gunnarsson, H.; Kaijser, B. Diffusion-in-Gel Enzyme-Linked Immunosorbent Assay for Routine Detection of IgG and IgM Antibodies to Campylobacter jejuni. *J. Infect. Dis.* **1983**, *148* (1), 82−92.
(70) Lehmann, S.; Seiffert, S.; Richtering, W. Spatially Resolved Tracer Diffusion in Complex Responsive Hydrogels. *J. Am. Chem. Soc.* **2012**, *134* (38), 15963−15969.
(71) Zustiak, S. P.; Boukari, H.; Leach, J. B. Solute Diffusion and Interactions in Cross-Linked Poly(Ethylene Glycol) Hydrogels Studied by Fluorescence Correlation Spectroscopy. *Soft Matter* **2010**, *6* (15), 3609−3618.
(72) Zhang, Q.; Wang, Y.; Mateescu, A.; Sergelen, K.; Kibrom, A.; Jonas, U.; Wei, T.; Dostalek, J. Biosensor based on hydrogel optical waveguide spectroscopy for the detection of 17β-estradiol. *Talanta* **2013**, *104*, 149−154.
(73) Luna Coronell, J. A.; Syed, P.; Sergelen, K.; Gyurján, I.; Weinhäusel, A. The current status of cancer biomarker research using tumour-associated antigens for minimal invasive and early cancer diagnostics. *J. Proteomics* **2012**, *76*, 102−115.
(74) Ziegenbalg, A.; Prados-Rosales, R.; Jenny-Avital, E. R.; Kim, R. S.; Casadevall, A.; Achkar, J. M. Immunogenicity of Mycobacterial Vesicles in Humans: Identification of a New Tuberculosis Antibody Biomarker. *Tuberculosis (Oxford, U. K.)* **2013**, *93* (4), 448−455.
(75) Han, M.; Nagele, E.; DeMarshall, C.; Acharya, N.; Nagele, R. Diagnosis of Parkinson's Disease Based on Disease-Specific Autoantibody Profiles in Human Sera. *PLoS One* **2012**, *7* (2), e32383.
(76) Scott, A. M.; Wolchok, J. D.; Old, L. J. Antibody therapy of cancer. *Nat. Rev. Cancer* **2012**, *12* (4), 278−287.
(77) Casadevall, A.; Pirofski, L.-A. Immunoglobulins in defense, pathogenesis and therapy of fungal diseases. *Cell Host Microbe* **2012**, *11* (5), 447−456.
(78) Woll, D. Fluorescence correlation spectroscopy in polymer science. *RSC Adv.* **2014**, *4* (5), 2447−2465.
(79) Li, M.; Cushing, S. K.; Wu, N. Plasmon-enhanced optical sensors: a review. *Analyst* **2015**, *140* (2), 386−406.
(80) Beines, P. W.; Klosterkamp, I.; Menges, B.; Jonas, U.; Knoll, W. Responsive Thin Hydrogel Layers from Photo-Cross-Linkable Poly-(N-isopropylacrylamide) Terpolymers. *Langmuir* **2007**, *23* (4), 2231−2238.
(81) Arnold, R. The titration of polymeric acids. *J. Colloid Sci.* **1957**, *12* (6), 549−556.
(82) Heitz, C.; Rawiso, M.; François, J. X-ray scattering study of a poly(methacrylic acid) sample as a function of its neutralization degree. *Polymer* **1999**, *40* (7), 1637−1650.
(83) Pohlmeier, A.; Haber-Pohlmeier, S. Ionization of short polymethacrylic acid: titration, DLS, and model calculations. *J. Colloid Interface Sci.* **2004**, *273* (2), 369−380.
(84) Nova, L.; Uhlik, F.; Kosovan, P. Local pH and effective pKA of weak polyelectrolytes - insights from computer simulations. *Phys. Chem. Chem. Phys.* **2017**, *19*, 14376.
(85) http://www.atdbio.com/content/34/Alexa-dyes.
(86) Fond, A. M.; Birenbaum, N. S.; Felton, E. J.; Reich, D. H.; Meyer, G. J. Preferential noncovalent immunoglobulin G adsorption onto hydrophobic segments of multi-functional metallic nanowires. *J. Photochem. Photobiol., A* **2007**, *186* (1), 57−64.
(87) Vagias, A.; Raccis, R.; Koynov, K.; Jonas, U.; Butt, H.-J.; Fytas, G.; Košovan, P.; Lenz, O.; Holm, C. Complex Tracer Diffusion Dynamics in Polymer Solutions. *Phys. Rev. Lett.* **2013**, *111* (8), 088301.
(88) Phillies, G. D. J.; Clomenil, D. Probe diffusion in polymer solutions under.THETA. and good conditions. *Macromolecules* **1993**, *26* (1), 167−170.
(89) Langevin, D.; Rondelez, F. Sedimentation of large colloidal particles through semidilute polymer solutions. *Polymer* **1978**, *19* (8), 875−882.
(90) Cai, L.-H.; Panyukov, S.; Rubinstein, M. Mobility of Nonsticky Nanoparticles in Polymer Liquids. *Macromolecules* **2011**, *44* (19), 7853−7863.
(91) Hawe, A.; Hulse, W. L.; Jiskoot, W.; Forbes, R. T. Taylor Dispersion Analysis Compared to Dynamic Light Scattering for the Size Analysis of Therapeutic Peptides and Proteins and Their Aggregates. *Pharm. Res.* **2011**, *28* (9), 2302−2310.
(92) Kapusta, P. Absolute Diffusion Coefficients: Compilation of Reference Data for FCS Calibration, Application note, PicoQuant GmbH.
(93) Rigler, R.; Elson, E. S. *Fluorescence Correlation Spectroscopy: Theory and Applications*; Springer: Berlin, 2001.

DOI: 10.1021/acs.macromol.7b00514
Macromolecules XXXX, XXX, XXX−XXX